

1 Catenin signaling controls phrenic motor neuron 2 development and function during a narrow temporal window

3 Alicia N. Vagnozzi¹, Matthew T. Moore¹, Raquel López de Boer¹, Aambar Agarwal¹, Niccolò
4 Zampieri², Lynn T. Landmesser¹, Polyxeni Philippidou¹

5

- 6 1. Department of Neurosciences, Case Western Reserve University, Cleveland, OH, USA
- 7 2. Max Delbrück Center for Molecular Medicine in the Helmholtz Association (MDC), Berlin,
8 Germany

9

10 Correspondence to: pxp282@case.edu

11

12 **Keywords:** cadherins, catenins, respiratory, phrenic motor neurons, breathing

13

14 Abstract

15 Phrenic Motor Column (PMC) neurons are a specialized subset of motor neurons (MNs)
16 that provide the only motor innervation to the diaphragm muscle and are therefore essential for
17 survival. Despite their critical role, the mechanisms that control phrenic MN development and
18 function are not well understood. Here, we show that catenin-mediated cadherin adhesive
19 function is required for multiple aspects of phrenic MN development. Deletion of β - and γ -
20 catenin from MN progenitors results in perinatal lethality and a severe reduction in phrenic MN
21 bursting activity. In the absence of catenin signaling, phrenic MN topography is eroded, MN
22 clustering is lost and phrenic axons and dendrites fail to grow appropriately. Despite the
23 essential requirement for catenins in early phrenic MN development, they appear to be
24 dispensable for phrenic MN maintenance, as catenin deletion from postmitotic MNs does not
25 impact phrenic MN topography or function. Our data reveal a fundamental role for catenins in
26 PMC development and suggest that distinct mechanisms are likely to control PMC
27 maintenance.

28

29 **Introduction**

30 Breathing is an essential motor behavior that is required for survival. In mammals,
31 contraction of the diaphragm muscle is critical for bringing oxygenated air into the lungs during
32 inspiration (Greer, 2012). Diaphragm contractions are mediated by a specialized subset of
33 motor neurons (MNs), Phrenic Motor Column (PMC) neurons that reside in the cervical spinal
34 cord and project their axons along the phrenic nerve in the thoracic cavity to reach the
35 diaphragm. Phrenic MNs exhibit distinct properties from other MN subtypes, including tight
36 clustering and stereotyped axonal and dendritic morphologies. While they are derived from a
37 common MN progenitor domain, phrenic MNs acquire their unique features through the activity
38 of a selective transcriptional program that distinguishes them from other MNs (Chaimowicz et
39 al., 2019; Machado et al., 2014; Philippidou et al., 2012; Vagozzi et al., 2020). Phrenic-specific
40 transcription factors (TFs) initiate and maintain the expression of a distinct set of genes,
41 including a unique combination of cell surface adhesion molecules (Machado et al., 2014;
42 Vagozzi et al., 2020). While many of these molecular markers show specific and sustained
43 expression in phrenic MNs, their functions in phrenic MN development and maintenance have
44 not been tested.

45 We previously identified a distinct combinatorial cadherin code that defines phrenic MNs,
46 which includes both the broadly expressed type I N-cadherin and a subset of specific type II
47 cadherins (Vagozzi et al., 2020). Cadherins are calcium-dependent transmembrane cell
48 adhesion molecules that interact with cytosolic catenin proteins to induce changes in the actin
49 cytoskeleton, thus regulating many neuronal processes such as migration, topography and
50 morphology (Seong et al., 2015). For example, cadherins regulate cortical neuron migration
51 (Martinez-Garay, 2020), hippocampal dendritic growth and branching (Bekirov et al., 2008; Esch
52 et al., 2000; Yu and Malenka, 2003), as well as dendrite morphogenesis and arborization within
53 the visual and olfactory systems (Duan et al., 2018; Hirano and Takeichi, 2012; Masai et al.,
54 2003; Riehl et al., 1996; Tanabe et al., 2006; Zhu and Luo, 2004). In the spinal cord, cadherins
55 engage β - and γ -catenins to establish the segregation and settling position of MN cell bodies
56 (Demireva et al., 2011; Dewitz et al., 2019; Dewitz et al., 2018; Price et al., 2002). β -catenin is
57 required in muscle for neuromuscular junction (NMJ) formation and function, however it appears
58 to act redundantly with γ -catenin in MNs, as only joint β - and γ -catenin inactivation leads to
59 disorganization of MN subtypes, including PMC neurons (Demireva et al., 2011; Li et al., 2008;
60 Vagozzi et al., 2020). However, it is unknown whether β - and γ -catenins have additional roles
61 in phrenic MN development and function, and whether they continue to be required after initial
62 PMC topography has been established.

63 Here, we show that catenin activity is required for proper respiratory behavior and robust
64 respiratory output. After MN-specific deletion of β - and γ -catenin, mice display severe
65 respiratory insufficiency, gasp for breath, and die within hours of birth. Using phrenic nerve
66 recordings, we determined that catenins are crucial for respiratory motor output, as MN-specific
67 catenin inactivation leads to a striking decrease in phrenic MN activity. We further show that
68 catenins are required to establish phrenic MN cell body settling position, as well as PMC axonal
69 and dendritic morphology. Finally, we show that catenins are only required for PMC
70 development and function during a narrow developmental window, as catenin deletion from
71 postmitotic MNs does not impact respiratory output. Our data demonstrate a fundamental role
72 for the cadherin-catenin cell adhesion complex in phrenic MN development and respiratory
73 function and indicate that distinct pathways likely act to maintain PMC function.

74 **Materials and Methods**

75 **Mouse genetics**

76 The β -catenin (Brault et al., 2001) and γ -catenin (Demireva et al., 2011) alleles,
77 *Olig2::Cre* (Dessaud et al., 2007) and *ChAT::Cre* (Lowell et al., 2006) lines were generated as
78 previously described and maintained on a mixed background. Mouse colony maintenance and
79 handling was performed in compliance with protocols approved by the Institutional Animal Care
80 Use Committee of Case Western Reserve University. Mice were housed in a 12-hour light/dark
81 cycle in cages containing no more than five animals at a time.

82 **Immunohistochemistry and in situ hybridization**

83 Immunohistochemistry was performed as previously described (Philippidou et al., 2012;
84 Vagnozzi et al., 2020), on tissue fixed for 2 hours in 4% paraformaldehyde (PFA) and
85 cryosectioned at 16 μ m. Wholemounts of diaphragm muscles were stained as described
86 (Philippidou et al., 2012). The following antibodies were used: goat anti-Scip (1:5000; Santa
87 Cruz Biotechnology, RRID:AB_2268536), mouse anti-Islet1/2 (1:1000, DSHB,
88 RRID:AB_2314683) (Tsuchida et al., 1994), rabbit anti-neurofilament (1:1000; Synaptic
89 Systems, RRID:AB_887743), rabbit anti-synaptophysin (1:250, Thermo Fisher,
90 RRID:AB_10983675), and α -bungarotoxin Alexa Fluor 555 conjugate (1:1000; Invitrogen,
91 RRID:AB_2617152). Images were obtained with a Zeiss LSM 800 confocal microscope and
92 analyzed with Zen Blue, ImageJ (Fiji), and Imaris (Bitplane). Phrenic MN number was quantified
93 using the Imaris “spots” function to detect cell bodies that coexpressed high levels of Scip and
94 Islet1/2 in a region of interest limited to the left and right sides of the ventral spinal cord.

95 **Dil tracing**

96 For labeling of phrenic MNs, crystals of carbocyanine dye, Dil (Invitrogen, #D3911) were
97 pressed onto the phrenic nerves of eviscerated embryos at e18.5, and the embryos were
98 incubated in 4% PFA at 37°C in the dark for 4-5 weeks. Spinal cords were then dissected,
99 embedded in 4% low melting point agarose (Invitrogen) and sectioned using a Leica VT1000S
100 vibratome at 100 to 150 μ m.

101 **Positional analysis**

102 MN positional analysis was performed as previously described (Dewitz et al., 2019;
103 Dewitz et al., 2018). MN positions were acquired using the “spots” function of the imaging
104 software Imaris (Bitplane) to assign x and y coordinates. Coordinates were expressed relative to
105 the midpoint of the spinal cord midline, defined as position x=0, y=0. To account for
106 experimental variations in spinal cord size, orientation, and shape, sections were normalized to
107 a standardized spinal cord whose dimensions were empirically calculated at e13.5 (midline to
108 the lateral edge=390 μ m). We analyzed every other section containing the entire PMC (20-30
109 sections in total per embryo).

110 **Dendritic orientation analysis**

111 For the analysis of dendritic orientation, we superimposed a radial grid divided into
112 eighths (45 degrees per octant) centered over phrenic MN cell bodies spanning the entire length
113 of the dendrites. We drew a circle around the cell bodies and deleted the fluorescence
114 associated with them. Fiji (ImageJ) was used to calculate the fluorescent intensity (IntDen) in
115 each octant which was divided by the sum of the total fluorescent intensity to calculate the
116 percentage of dendritic intensity in each area.

117 **Electrophysiology**

118 Electrophysiology was performed as previously described (Vagnozzi et al., 2020). Mice
119 were cryoanesthetized and rapid dissection was carried out in 22-26°C oxygenated Ringer's
120 solution. The solution was composed of 128mM NaCl, 4mM KCl, 21mM NaHCO₃, 0.5mM
121 NaH₂PO₄, 2mM CaCl₂, 1mM MgCl₂, and 30mM D-glucose and was equilibrated by bubbling in
122 95% O₂/5% CO₂. The hindbrain and spinal cord were exposed by ventral laminectomy, and
123 phrenic nerves exposed and dissected free of connective tissue. A transection at the
124 pontomedullary boundary rostral to the anterior inferior cerebellar artery was used to initiate
125 fictive inspiration. Electrophysiology was performed under continuous perfusion of oxygenated
126 Ringer's solution from rostral to caudal. Suction electrodes were attached to phrenic nerves just
127 proximal to their arrival at the diaphragm. The signal was band-pass filtered from 10Hz to 3kHz
128 using AM-Systems amplifiers (Model 3000), amplified 5,000-fold, and sampled at a rate of
129 50kHz with a Digidata 1440A (Molecular Devices). Data were recorded using AxoScope
130 software (Molecular Devices) and analyzed in Spike2 (Cambridge Electronic Design). Burst
131 duration and burst activity were computed from 4-5 bursts per mouse, while burst frequency
132 was determined from 10 or more minutes of recording time per mouse. Burst activity was
133 computed by rectifying and integrating the traces with an integration time equal to 2 seconds,
134 long enough to encompass the entire burst. The maximum amplitude of the rectified and
135 integrated signal was then measured and reported as the total burst activity.

136 **Plethysmography**

Conscious, unrestrained P0 mice were placed in a whole body, flow-through plethysmograph (emka) attached to a differential pressure transducer (emka). We modified 10ml syringes to use as chambers, as smaller chambers increase signal detection in younger mice. Experiments were done in room air (79% nitrogen, 21% oxygen). Mice were placed in the chamber for 30 seconds at a time, for a total of three to five times, and breathing parameters were recorded. Mice were directly observed to identify resting breaths. At least ten resting breaths were analyzed from every mouse. Data are presented as fold control, where the control is the average of 2 littermates in normal air.

145 Experimental design and statistical analysis

146 For all experiments a minimum of three embryos per genotype, both male and female,
147 were used for all reported results unless otherwise stated. The Shapiro-Wilk test was used to
148 determine normality. All data, with the exception of electrophysiology burst activity data in
149 figures 2 and 6, showed normal distribution and p-values were calculated using unpaired, two-
150 tailed Student's *t* test. Burst activity data in figures 2 and 6 showed non-normal distribution and
151 p-values were calculated using the Mann-Whitney test. $p < 0.05$ was considered to be
152 statistically significant, where * $p < 0.05$, ** $p < 0.01$, *** $p < 0.001$, and **** $p < 0.0001$. Data are
153 presented as box and whisker plots with each dot representing data from one mouse unless
154 otherwise stated. Small open squares in box and whisker plots represent the mean.

155 **Results**

156 Catenin signaling is required for survival, proper respiratory behavior and phrenic MN
157 activation

158 Phrenic MNs express a distinct combinatorial cadherin code (Machado et al., 2014;
159 Vagnozzi et al., 2020), but the collective contribution of these molecules to phrenic MN
160 development, maintenance and function has not been established. We previously found that
161 phrenic MNs express the type I *N-cadherin* (*N-cad*) and the type II cadherins *Cdh6*, 9, 10, 11,
162 and 22 (Vagnozzi et al., 2020). To investigate the role of cadherin signaling in phrenic MN

163 development, we eliminated cadherin signaling in MN progenitors by inactivating β - and γ -
164 *catenin* using a *Olig2::Cre* promoter (β -*catenin* *flx/flox*; γ -*catenin* *flx/flox*; *Olig2::Cre*, referred
165 to as $\beta\gamma$ -*cat*^{MNA} mice). β - and γ -catenin are obligate intracellular factors required for cadherin-
166 mediated cell adhesive function and catenin deletion enables us to interrogate the full repertoire
167 of cadherin actions in phrenic MNs (Figure 1a). We find that $\beta\gamma$ -*cat*^{MNA} mice are born alive but
168 die within 24 hours of birth and often display severe flexion of the wrist joint (Figure 1b).

169 In order to assess breathing in $\beta\gamma$ -*cat*^{MNA} mice, we utilized unrestrained whole body flow-
170 through plethysmography at postnatal day (P)0 (Figure 1c). We found that $\beta\gamma$ -*cat*^{MNA} mice have
171 a 45% reduction in tidal volume (the amount of air inhaled during a normal breath), while
172 respiratory frequency is not affected (Figure 1d-e). This results in an average 45% reduction in
173 overall air drawn into the lungs per minute (minute ventilation, figure 1e), indicating $\beta\gamma$ -*cat*^{MNA}
174 mice likely die from respiratory failure. Our findings indicate that catenin signaling is necessary
175 for proper respiratory behavior and survival. To further examine respiratory circuitry intrinsic to
176 the brainstem and spinal cord, we performed suction recordings of the phrenic nerve in isolated
177 brainstem-spinal cord preparations (Figure 2a). These preparations display fictive inspiration
178 after the removal of inhibitory networks in the pons via transection, and thus represent a robust
179 model to interrogate circuit level changes. We examined whether catenin deletion impacts
180 circuit output at embryonic day (e)18.5/P0, shortly before $\beta\gamma$ -*cat*^{MNA} mice die. We observed a
181 striking reduction in the activation of phrenic MNs in $\beta\gamma$ -*cat*^{MNA} mice (Figure 2b). While bursts in
182 control mice exhibit large peak amplitude, bursts in $\beta\gamma$ -*cat*^{MNA} mice were either of very low
183 amplitude (~85%) or non-detectable (~15%). After rectifying and integrating the traces, we
184 found a nearly 70% decrease in total burst activity in $\beta\gamma$ -*cat*^{MNA} mice (Figure 2c). Our data
185 indicate that cadherin signaling is imperative for robust activation of phrenic MNs during
186 inspiration.

187 **Catenins establish phrenic MN topography and organization**

188 What accounts for the loss of phrenic MN activity in $\beta\gamma$ -*cat*^{MNA} mice? We asked whether
189 early phrenic MN specification, migration and survival are impacted after catenin inactivation.
190 We acquired transverse spinal cord sections through the entire PMC at e13.5 and stained for
191 the phrenic-specific TF Scip and the MN-specific TF *Isl1/2*, to label all phrenic MNs. We found a
192 cluster of Scip+ MNs in the ventral cervical spinal cord of both control and $\beta\gamma$ -*cat*^{MNA} mice,
193 indicating that early phrenic MN specification is unperturbed (Figure 3a). However, we observed
194 a significant reduction in phrenic MN numbers in $\beta\gamma$ -*cat*^{MNA} mice, indicating that catenin
195 signaling is necessary for phrenic MN survival (Figure 3b).

196 While phrenic MNs are normally distributed along the rostrocaudal axis, we found that
197 they sometimes show migratory defects, where several phrenic MNs remain close to the midline
198 instead of fully migrating (Figure 3c, arrow), and also appear to shift both ventrally and medially
199 in $\beta\gamma$ -*cat*^{MNA} mice. To quantitate PMC cell body position, each phrenic MN was assigned a
200 cartesian coordinate, with the midpoint of the spinal cord midline defined as (0,0). $\beta\gamma$ -*cat*^{MNA}
201 mice displayed a significant shift in phrenic MN cell body position, with cell bodies shifting
202 ventrally towards the edge of the spinal cord and towards the midline (Figure 3c-f). We
203 quantified the average ventrodorsal and mediolateral phrenic MN position per embryo and found
204 a significant change in phrenic MN position in both axes in $\beta\gamma$ -*cat*^{MNA} mice (Figure 3g).
205 Correlation analysis indicated that control and $\beta\gamma$ -*cat*^{MNA} mice are dissimilar from each other
206 ($r=0.47$, Figure 3h), indicating that catenins establish phrenic MN coordinates during
207 development.

208 In addition to changes in cell body position, we also noticed that phrenic MNs appear to
209 lose their tight clustering in $\beta\gamma\text{-cat}^{\text{MNA}}$ mice. PMC clustering is thought to be critical for the proper
210 development of the respiratory system because it facilitates recruitment of motor units through
211 electrical coupling in the embryo to compensate for weak inspiratory drive (Greer and Funk,
212 2005). In order to determine PMC clustering defects, we used Imaris to measure the average
213 distance between phrenic MNs. We found that $\beta\gamma\text{-cat}^{\text{MNA}}$ mice had a nearly 50% increase in the
214 average distance between neighboring cells (Figure 3i), indicating that the cadherin/catenin
215 adhesive complex contributes to the formation of a tightly clustered phrenic motor column.

216 **Catenins are required for phrenic MN dendrite and axon growth**

217 Since cadherin/catenin signaling is imperative for phrenic MN organization, we also
218 asked whether any other aspects of phrenic MN development, such as dendritic and axon
219 growth, might rely on catenin actions. We examined dendritic orientation in control and $\beta\gamma\text{-cat}^{\text{MNA}}$
220 mice by injecting the lipophilic dye dil into the phrenic nerve at e18.5 (Figure 4a). Dil
221 diffuses along the phrenic nerve to label both PMC cell bodies and dendrites. Consistent with
222 our earlier observations, we found that phrenic cell bodies are often scattered in $\beta\gamma\text{-cat}^{\text{MNA}}$ mice.
223 Interestingly, even phrenic MNs that are significantly displaced correctly project along the
224 phrenic nerve (arrows, figure 4a), indicating that changes in cell body position do not impact
225 axon trajectory choice. In control mice, phrenic MN dendrites branch out in dorsolateral to
226 ventromedial directions; in $\beta\gamma\text{-cat}^{\text{MNA}}$ mice, however, they exhibit stunted growth, defasciculation
227 and a failure to extend in the dorsolateral direction (Figure 4a).

228 To quantify these changes, we superimposed a radial grid divided into octants onto the
229 dendrites and measured the fluorescent intensity in each octant after removal of any
230 fluorescence associated with the cell bodies. Zero degrees was defined by a line running
231 perpendicular from the midline through the center of cell bodies. In control mice, the majority of
232 dendrites project in the dorsolateral direction (0-90 degrees), representing 40-45% of the overall
233 dendritic intensity (Figure 4b, d, e). Ventrally projecting dendrites (180-225 degrees and 315-
234 360 degrees) were also prominent, giving rise to nearly 30% of the overall dendritic intensity
235 (Figure 4b, d, e). We found that catenin deletion resulted in a striking reduction in dorsolateral
236 dendrites, together with a significant increase in ventral dendrites (Figure 4c-e), indicating that
237 cadherins are necessary for establishing phrenic MN dendritic orientation. These changes in
238 phrenic dendritic topography in $\beta\gamma\text{-cat}^{\text{MNA}}$ mice may impact their targeting by respiratory
239 populations in the brainstem, leading to the reduction in phrenic MN activation observed.

240 We then asked whether catenins might also play an analogous role in phrenic axon
241 extension and arborization. We examined diaphragm innervation in control and $\beta\gamma\text{-cat}^{\text{MNA}}$ mice
242 at e18.5. We found that $\beta\gamma\text{-cat}^{\text{MNA}}$ mice display a lack of innervation in the ventral diaphragm
243 (Figure 5a, arrow), while the parts of the diaphragm that are innervated show a reduction in
244 terminal arborization complexity (Figure 5a, star). Quantitation of total phrenic projections
245 revealed a significant reduction in overall diaphragm innervation (Figure 5b-c). Collectively our
246 data point to a catenin requirement for phrenic MN topography and axon and dendrite
247 arborization, suggesting that these changes in early phrenic MN development lead to loss of
248 phrenic MN activity and perinatal lethality due to respiratory insufficiency.

249 **A narrow temporal requirement for catenin signaling in phrenic MN topography and
250 function.**

251 Given the essential role for catenins in early phrenic MN development, we wanted to
252 further understand the temporal dynamics of cadherin signaling, and asked whether sustained

253 catenin expression is required for maintenance of the respiratory circuit. We used a *ChAT::Cre*
254 promoter to specifically delete β - and γ -catenin in postmitotic MNs (β -catenin *flox/flox*; γ -catenin
255 *flox/flox*; *ChAT::Cre*, referred to as $\beta\gamma\text{-cat}^{\text{ChATMN}\Delta}$ mice). $\beta\gamma\text{-cat}^{\text{ChATMN}\Delta}$ mice survive to adulthood
256 and do not display respiratory insufficiency or gasping at birth. We first assessed cell body
257 position and found no changes between control and $\beta\gamma\text{-cat}^{\text{ChATMN}\Delta}$ mice (Figure 6a). Injecting dil
258 into the phrenic nerve also revealed no differences in dendritic orientation between control and
259 $\beta\gamma\text{-cat}^{\text{ChATMN}\Delta}$ mice (Figure 6b). To assess respiratory circuit function, we performed phrenic
260 nerve recordings in isolated brainstem-spinal cord preparations in control and $\beta\gamma\text{-cat}^{\text{ChATMN}\Delta}$
261 mice at P4, and found that $\beta\gamma\text{-cat}^{\text{ChATMN}\Delta}$ mice exhibit similar phrenic MN bursting frequency,
262 burst duration and overall activity as control mice (Figure 6c-d). Our data suggests that
263 cadherins engage catenin signaling during a short temporal window early in development to
264 shape respiratory motor output, but appear to be dispensable once early phrenic MN
265 topography and morphology have been established.

266

267 Discussion

268 Phrenic MNs are a critical neuronal population that is essential for breathing, yet the
269 molecular mechanisms that control their development and maintenance have remained elusive.
270 Here, we show that catenin-mediated cadherin adhesive function is required for phrenic MN
271 organization, axonal and dendritic arborization, and respiratory output during a narrow
272 developmental window. While catenins have a critical role in early phrenic MN development,
273 they appear to be dispensable for maintaining the morphology and function of these MNs. Our
274 findings indicate that distinct molecular pathways are likely to mediate the establishment and
275 maintenance of respiratory motor circuits at different timepoints throughout development and
276 adulthood.

277

278 Catenins appear to be critical for phrenic MN organization. We find that catenin
279 inactivation leads to both ventral shifts in PMC position and loss of clustering between cell
280 bodies. While we observe similar shifts in cell body position when we inactivate 4 out of the 6
281 cadherins expressed in PMC neurons (cadherins N, 6, 9 and 10- $N^{\text{MN}\Delta}6910^{-/-}$ mice), we do not
282 see a loss of clustering in these mice (Vagnozzi, 2022). This could suggest that retaining
283 expression of the remaining PMC-specific cadherins, 11 and 22, is sufficient to maintain the
284 phrenic MN distinct tight clustering organization. Alternatively, our data could indicate that cell
285 non-autonomous cadherin function plays a predominant role in MN clustering, and that
286 eliminating cadherin signaling from all MNs leads to scattering and mixing of MN populations,
287 causing disorganization not seen when solely eliminating PMC-specific cadherins. Despite
288 differentially affecting PMC clustering, we observe similar changes in phrenic MN activity in
289 $N^{\text{MN}\Delta}6910^{-/-}$ and $\beta\gamma\text{-cat}^{\text{MN}\Delta}$ mice, suggesting that MN clustering may not significantly contribute to
290 phrenic MN activity. Alternatively, since the loss of activity we observe in both mouse models is
291 so severe, it may mask a subtler impact of clustering to PMC activity patterning and
292 synchronization. Decoupling PMC clustering from changes in neuronal morphology and cell
293 adhesion loss will help distinguish the contribution of each of these properties to respiratory
294 motor output.

295

296 Our data show that cadherin signaling is required both for the elaboration of PMC axons
297 and dendrites, however the impact of catenin inactivation on dendrites appears to be more
298 severe. Phrenic MNs are able to elaborate axons in $\beta\gamma\text{-cat}^{\text{MN}\Delta}$ mice and axonal topography and

299 orientation are mostly preserved, with some minor loss of terminal arborization. Dendrites
300 however appear to be severely stunted, project haphazardly and their topography is lost. This
301 indicates that cadherins have a much more predominant role in dendritic rather than axonal
302 elaboration. While many signaling pathways contribute to phrenic axon growth and diaphragm
303 innervation, including HGF/MET (Sefton et al., 2022), Slit/Robo (Charoy et al., 2017) and
304 Col25a1 (Tanaka et al., 2014), to our knowledge, cadherins are the first cell adhesion molecules
305 to be implicated in phrenic MN dendritic development.

306

307 Loss of catenin-mediated cadherin adhesive function results in a dramatic reduction of
308 phrenic MN activity that leads to perinatal lethality. This could be due to the loss of descending
309 inputs from brainstem respiratory centers that provide excitatory drive to initiate diaphragm
310 contraction during inhalation. The dramatic change in PMC dendritic coordinates is likely to
311 contribute significantly to the loss of presynaptic inputs and respiratory activity. Dendrites
312 represent the largest surface area of neurons, and thus receive the majority of synaptic input. In
313 sensory-motor circuits, proprioceptive inputs are primarily located on the dendrites of motor
314 neurons, and different motor pools exhibit distinct, stereotyped patterns of dendritic arborization
315 that contribute to sensory-motor specific connectivity (Balaskas et al., 2019; Vrieseling and
316 Arber, 2006). This mode of cadherin action in respiratory circuits would be consistent with
317 cadherin-dependent targeting mechanisms in the retina, where combinatorial codes of cadherin
318 expression serve to direct axons and dendrites of synaptically connected neurons to their
319 correct laminar targets (Duan et al., 2014; Duan et al., 2018; Osterhout et al., 2011).

320

321 In addition to establishing phrenic MN dendritic morphology, cadherins could directly
322 contribute to phrenic connectivity through establishing a molecular recognition program between
323 phrenic MN dendrites and pre-motor axons. Due to their restricted and selective expression in
324 neural populations, cadherins are thought to function in circuit assembly by dictating synaptic
325 specificity. Cadherin expression often reflects the functional connections formed in a circuit,
326 suggesting they may represent a molecular code dictating the formation of selective synaptic
327 connections (Suzuki et al., 1997). Cadherins are expressed on dendrites, axons, and growth
328 cones of developing neurons (Basu et al., 2015) and have been visualized at synapses in both
329 pre and postsynaptic compartments (Bartelt-Kirbach et al., 2010; Benson and Tanaka, 1998;
330 Bozdagi et al., 2000; Fannon and Colman, 1996; Manabe et al., 2000; Suzuki et al., 2007;
331 Uchida et al., 1996; Yamagata et al., 1995). Therefore, cadherins could function to establish
332 respiratory neuron connectivity independently of their role in dictating axonal and dendritic
333 targeting, at the level of the synapse, as it has been described in the hippocampus (Basu et al.,
334 2017; Williams et al., 2011). Future experiments will determine the primary mode of cadherin
335 action in respiratory circuit formation.

336

337 While early cadherin inactivation in MN progenitors results in dramatic changes in
338 phrenic MN morphology and activity and leads to perinatal death, cadherin inactivation in
339 postmitotic MNs does not impact respiratory output. This result provides initial evidence
340 supporting a predominant role for cadherins in shaping dendritic orientation, as they appear to
341 be dispensable once phrenic MN morphology has been established. Our findings indicate a
342 model in which cadherins may function to direct the dendrites and axons of pre and
343 postsynaptic neurons to the correct location, while additional cell adhesion molecules dictate
344 synaptic connectivity. In support of this hypothesis, we have identified a number of cell adhesion
345 molecules that are specifically expressed in phrenic MNs but are not required for their

346 morphology. Our results also indicate that distinct mechanisms may function to maintain
347 respiratory circuit integrity after initial formation. Understanding how these critical circuits are
348 maintained in adulthood is essential, as loss of respiratory function underlies lethality in many
349 neurodegenerative diseases such as Amyotrophic Lateral Sclerosis (ALS).

350

351 **Acknowledgements**

352 We thank Heather Broihier, Evan Deneris, Ashleigh Schaffer, Helen Miranda, and
353 members of the Philippidou lab for helpful discussions. This work was funded by NIH
354 R01NS114510 to PP, F30HD096788 to ANV, T32GM007250 to ANV/CWRU MSTP, and
355 F31NS124240 to MTM. PP is the Weidenthal Family Designated Professor in Career
356 Development.

357

358 **References**

359

360 Balaskas, N., Abbott, L.F., Jessell, T.M., and Ng, D. (2019). Positional Strategies for Connection
361 Specificity and Synaptic Organization in Spinal Sensory-Motor Circuits. *Neuron*.

362 Bartelt-Kirbach, B., Langer-Fischer, K., and Golenhofen, N. (2010). Different regulation of N-
363 cadherin and cadherin-11 in rat hippocampus. *Cell Commun Adhes* 17, 75-82.

364 Basu, R., Duan, X., Taylor, M.R., Martin, E.A., Muralidhar, S., Wang, Y., Gangi-Wellman, L.,
365 Das, S.C., Yamagata, M., West, P.J., *et al.* (2017). Heterophilic Type II Cadherins Are Required
366 for High-Magnitude Synaptic Potentiation in the Hippocampus. *Neuron* 96, 160-176 e168.

367 Basu, R., Taylor, M.R., and Williams, M.E. (2015). The classic cadherins in synaptic specificity.
368 *Cell Adh Migr* 9, 193-201.

369 Bekirov, I.H., Nagy, V., Svoronos, A., Huntley, G.W., and Benson, D.L. (2008). Cadherin-8 and
370 N-cadherin differentially regulate pre- and postsynaptic development of the hippocampal mossy
371 fiber pathway. *Hippocampus* 18, 349-363.

372 Benson, D.L., and Tanaka, H. (1998). N-cadherin redistribution during synaptogenesis in
373 hippocampal neurons. *J Neurosci* 18, 6892-6904.

374 Bozdagi, O., Shan, W., Tanaka, H., Benson, D.L., and Huntley, G.W. (2000). Increasing
375 numbers of synaptic puncta during late-phase LTP: N-cadherin is synthesized, recruited to
376 synaptic sites, and required for potentiation. *Neuron* 28, 245-259.

377 Brault, V., Moore, R., Kutsch, S., Ishibashi, M., Rowitch, D.H., McMahon, A.P., Sommer, L.,
378 Boussadia, O., and Kemler, R. (2001). Inactivation of the beta-catenin gene by Wnt1-Cre-
379 mediated deletion results in dramatic brain malformation and failure of craniofacial development.
380 *Development* 128, 1253-1264.

381 Chaimowicz, C., Ruffault, P.L., Cheret, C., Woehler, A., Zampieri, N., Fortin, G., Garratt, A.N.,
382 and Birchmeier, C. (2019). Teashirt1 (Tshz1) is essential for the development, survival and
383 function of hypoglossal and phrenic motor neurons. *Development*.

384 Charoy, C., Dinvaut, S., Chaix, Y., Morle, L., Sanyas, I., Bozon, M., Kindbeiter, K., Durand, B.,
385 Skidmore, J.M., De Groef, L., *et al.* (2017). Genetic specification of left-right asymmetry in the
386 diaphragm muscles and their motor innervation. *Elife* 6.

387 Demireva, E.Y., Shapiro, L.S., Jessell, T.M., and Zampieri, N. (2011). Motor neuron position and
388 topographic order imposed by beta- and gamma-catenin activities. *Cell* 147, 641-652.

389 Dessaud, E., Yang, L.L., Hill, K., Cox, B., Ulloa, F., Ribeiro, A., Mynett, A., Novitch, B.G., and
390 Briscoe, J. (2007). Interpretation of the sonic hedgehog morphogen gradient by a temporal
391 adaptation mechanism. *Nature* 450, 717-720.

392 Dewitz, C., Duan, X., and Zampieri, N. (2019). Organization of motor pools depends on the
393 combined function of N-cadherin and type II cadherins. *Development* **146**.

394 Dewitz, C., Pimpinella, S., Hackel, P., Akalin, A., Jessell, T.M., and Zampieri, N. (2018). Nuclear
395 Organization in the Spinal Cord Depends on Motor Neuron Lamination Orchestrated by Catenin
396 and Afadin Function. *Cell Rep* **22**, 1681-1694.

397 Duan, X., Krishnaswamy, A., De la Huerta, I., and Sanes, J.R. (2014). Type II cadherins guide
398 assembly of a direction-selective retinal circuit. *Cell* **158**, 793-807.

399 Duan, X., Krishnaswamy, A., Laboulaye, M.A., Liu, J., Peng, Y.R., Yamagata, M., Toma, K., and
400 Sanes, J.R. (2018). Cadherin Combinations Recruit Dendrites of Distinct Retinal Neurons to a
401 Shared Interneuronal Scaffold. *Neuron* **99**, 1145-1154 e1146.

402 Esch, T., Lemmon, V., and Bunker, G. (2000). Differential effects of NgCAM and N-cadherin on
403 the development of axons and dendrites by cultured hippocampal neurons. *J Neurocytol* **29**,
404 215-223.

405 Fannon, A.M., and Colman, D.R. (1996). A model for central synaptic junctional complex
406 formation based on the differential adhesive specificities of the cadherins. *Neuron* **17**, 423-434.

407 Greer, J.J. (2012). Control of breathing activity in the fetus and newborn. *Compr Physiol* **2**,
408 1873-1888.

409 Hirano, S., and Takeichi, M. (2012). Cadherins in brain morphogenesis and wiring. *Physiol Rev*
410 **92**, 597-634.

411 Li, X.M., Dong, X.P., Luo, S.W., Zhang, B., Lee, D.H., Ting, A.K., Neiswender, H., Kim, C.H.,
412 Carpenter-Hyland, E., Gao, T.M., *et al.* (2008). Retrograde regulation of motoneuron
413 differentiation by muscle beta-catenin. *Nat Neurosci* **11**, 262-268.

414 Lowell, B., Olson, D., and Yu, J. (2006). Development and phenotype of ChAT-IRES-Cre mice.
415 MGI Direct Data Submission.

416 Machado, C.B., Kanning, K.C., Kreis, P., Stevenson, D., Crossley, M., Nowak, M., Iacovino, M.,
417 Kyba, M., Chambers, D., Blanc, E., *et al.* (2014). Reconstruction of phrenic neuron identity in
418 embryonic stem cell-derived motor neurons. *Development* **141**, 784-794.

419 Manabe, T., Togashi, H., Uchida, N., Suzuki, S.C., Hayakawa, Y., Yamamoto, M., Yoda, H.,
420 Miyakawa, T., Takeichi, M., and Chisaka, O. (2000). Loss of cadherin-11 adhesion receptor
421 enhances plastic changes in hippocampal synapses and modifies behavioral responses. *Mol
422 Cell Neurosci* **15**, 534-546.

423 Martinez-Garay, I. (2020). Molecular Mechanisms of Cadherin Function During Cortical
424 Migration. *Front Cell Dev Biol* **8**, 588152.

425 Masai, I., Lele, Z., Yamaguchi, M., Komori, A., Nakata, A., Nishiwaki, Y., Wada, H., Tanaka, H.,
426 Nojima, Y., Hammerschmidt, M., *et al.* (2003). N-cadherin mediates retinal lamination,
427 maintenance of forebrain compartments and patterning of retinal neurites. *Development* 130,
428 2479-2494.

429 Osterhout, J.A., Josten, N., Yamada, J., Pan, F., Wu, S.W., Nguyen, P.L., Panagiotakos, G.,
430 Inoue, Y.U., Egusa, S.F., Volgyi, B., *et al.* (2011). Cadherin-6 mediates axon-target matching in
431 a non-image-forming visual circuit. *Neuron* 71, 632-639.

432 Philippidou, P., Walsh, C.M., Aubin, J., Jeannotte, L., and Dasen, J.S. (2012). Sustained Hox5
433 gene activity is required for respiratory motor neuron development. *Nat Neurosci* 15, 1636-1644.

434 Price, S.R., De Marco Garcia, N.V., Ranscht, B., and Jessell, T.M. (2002). Regulation of motor
435 neuron pool sorting by differential expression of type II cadherins. *Cell* 109, 205-216.

436 Riehl, R., Johnson, K., Bradley, R., Grunwald, G.B., Cornel, E., Lilienbaum, A., and Holt, C.E.
437 (1996). Cadherin function is required for axon outgrowth in retinal ganglion cells in vivo. *Neuron*
438 17, 837-848.

439 Sefton, E.M., Gallardo, M., Tobin, C.E., Collins, B.C., Colasanto, M.P., Merrell, A.J., and
440 Kardon, G. (2022). Fibroblast-derived Hgf controls recruitment and expansion of muscle during
441 morphogenesis of the mammalian diaphragm. *Elife* 11.

442 Seong, E., Yuan, L., and Arikkath, J. (2015). Cadherins and catenins in dendrite and synapse
443 morphogenesis. *Cell Adh Migr* 9, 202-213.

444 Suzuki, S.C., Furue, H., Koga, K., Jiang, N., Nohmi, M., Shimazaki, Y., Katoh-Fukui, Y.,
445 Yokoyama, M., Yoshimura, M., and Takeichi, M. (2007). Cadherin-8 is required for the first relay
446 synapses to receive functional inputs from primary sensory afferents for cold sensation. *J
447 Neurosci* 27, 3466-3476.

448 Suzuki, S.C., Inoue, T., Kimura, Y., Tanaka, T., and Takeichi, M. (1997). Neuronal circuits are
449 subdivided by differential expression of type-II classic cadherins in postnatal mouse brains. *Mol
450 Cell Neurosci* 9, 433-447.

451 Tanabe, K., Takahashi, Y., Sato, Y., Kawakami, K., Takeichi, M., and Nakagawa, S. (2006).
452 Cadherin is required for dendritic morphogenesis and synaptic terminal organization of retinal
453 horizontal cells. *Development* 133, 4085-4096.

454 Tanaka, T., Wakabayashi, T., Oizumi, H., Nishio, S., Sato, T., Harada, A., Fujii, D., Matsuo, Y.,
455 Hashimoto, T., and Iwatsubo, T. (2014). CLAC-P/collagen type XXV is required for the
456 intramuscular innervation of motoneurons during neuromuscular development. *J Neurosci* 34,
457 1370-1379.

458 Tsuchida, T., Ensini, M., Morton, S.B., Baldassare, M., Edlund, T., Jessell, T.M., and Pfaff, S.L.
459 (1994). Topographic organization of embryonic motor neurons defined by expression of LIM
460 homeobox genes. *Cell* 79, 957-970.

461 Uchida, N., Honjo, Y., Johnson, K.R., Wheelock, M.J., and Takeichi, M. (1996). The
462 catenin/cadherin adhesion system is localized in synaptic junctions bordering transmitter
463 release zones. *J Cell Biol* 135, 767-779.

464 Vagnozzi, A.N., Garg, K., Dewitz, C., Moore, M.T., Cregg, J.M., Jeannotte, L., Zampieri, N.,
465 Landmesser, L.T., and Philippidou, P. (2020). Phrenic-specific transcriptional programs shape
466 respiratory motor output. *Elife* 9.

467 Vagnozzi, A.N, et al. (2022). Coordinated cadherin functions sculpt respiratory motor circuit
468 connectivity. *bioRxiv*.

469 Vrieseling, E., and Arber, S. (2006). Target-induced transcriptional control of dendritic patterning
470 and connectivity in motor neurons by the ETS gene Pea3. *Cell* 127, 1439-1452.

471 Williams, M.E., Wilke, S.A., Daggett, A., Davis, E., Otto, S., Ravi, D., Ripley, B., Bushong, E.A.,
472 Ellisman, M.H., Klein, G., et al. (2011). Cadherin-9 regulates synapse-specific differentiation in
473 the developing hippocampus. *Neuron* 71, 640-655.

474 Yamagata, M., Herman, J.P., and Sanes, J.R. (1995). Lamina-specific expression of adhesion
475 molecules in developing chick optic tectum. *J Neurosci* 15, 4556-4571.

476 Yu, X., and Malenka, R.C. (2003). Beta-catenin is critical for dendritic morphogenesis. *Nat*
477 *Neurosci* 6, 1169-1177.

478 Zhu, H., and Luo, L. (2004). Diverse functions of N-cadherin in dendritic and axonal terminal
479 arborization of olfactory projection neurons. *Neuron* 42, 63-75.

480

481

482 **Figure legends**

483 **Figure 1. Catenin signaling is required for survival and proper respiratory behavior**

484 **a)** B- and γ -catenin are obligate intracellular factors required for cadherin-mediated cell
485 adhesive function. We utilized inactivation of β - and γ -catenin in MNs (β -catenin flx/flx ; γ -
486 catenin flx/flx ; *Olig2::Cre*, referred to as $\beta\gamma$ -cat MNA mice) as a strategy to define the function of
487 cadherin signaling in phrenic MNs. **b)** Appearance of P0 control and $\beta\gamma$ -cat MNA mice. $\beta\gamma$ -cat MNA
488 mice are cyanotic and die shortly after birth. **c)** Experimental setup for whole body
489 plethysmography experiments. **d)** Representative 10 second traces in room air from control and
490 $\beta\gamma$ -cat MNA mice at P0. **e)** $\beta\gamma$ -cat MNA mice display reduced tidal volume resulting in a 45%
491 reduction in overall ventilation (n=4 control, n=6 $\beta\gamma$ -cat MNA mice).

492 **Figure 2. Catenin signaling controls phrenic MN activation**

493 **a)** Schematic of brainstem-spinal cord preparation, which displays fictive inspiration after
494 removal of the pons. Suction electrode recordings were taken from the phrenic nerve in the
495 thoracic cavity at e18.5/P0. **b)** Enlargement of single respiratory bursts reveals a reduction in
496 burst amplitude and overall activity in $\beta\gamma$ -cat MNA mice. Partial (initial 350ms) bursts are shown.
497 While 85% of $\beta\gamma$ -cat MNA mice display respiratory bursts, 15% show no bursts throughout the
498 recording period. **c)** $\beta\gamma$ -cat MNA mice exhibit nearly 70% reduction in burst activity (n=10 control,
499 n=10 $\beta\gamma$ -cat MNA mice).

500 **Figure 3. Catenins establish phrenic MN topography and organization**

501 **a)** Rostral to caudal distribution of e13.5 phrenic MN cell bodies (yellow, defined by the
502 expression of Scip in green and *Isl1/2* in red) in control and $\beta\gamma$ -cat MNA mice. While phrenic MN
503 cell bodies in control mice gradually shift towards more ventral positions at caudal locations,
504 phrenic cell bodies are located ventrally in $\beta\gamma$ -cat MNA mice even at rostral levels. In addition, cell
505 bodies in $\beta\gamma$ -cat MNA mice appear less clustered. **b)** Reduction in phrenic MN number in $\beta\gamma$ -cat MNA
506 mice. **c)** Reconstructed distribution of cell bodies in control and $\beta\gamma$ -cat MNA mice. Occasional cell
507 bodies remain near the progenitor zone in $\beta\gamma$ -cat MNA mice (arrow), while others seem to be
508 dragged out of the spinal cord by their axon (arrowhead). **d)** Contour density plot of phrenic cell
509 body position in control and $\beta\gamma$ -cat MNA mice at e13.5. V-D μ m; ventrodorsal position, M-L μ m;
510 mediolateral position. (0,0) represents the center of the spinal cord in both dimensions. **e-f)**
511 Density plots of ventrodorsal (e) and mediolateral (f) cell body position in control and $\beta\gamma$ -cat MNA
512 mice. **g)** Quantification of ventrodorsal and mediolateral position, showing significant shifts in
513 $\beta\gamma$ -cat MNA mice. **h)** Correlation analysis of phrenic MN positional coordinates in control and $\beta\gamma$ -
514 cat MNA mice. 0 is no correlation, while 1 is a perfect correlation. **i)** Phrenic MNs have an
515 increased average distance to their neighboring phrenic MNs in $\beta\gamma$ -cat MNA mice, indicating loss
516 of clustering. Scale bar= 25 μ m.

517 **Figure 4. Catenins control phrenic MN dendritic growth and orientation**

518 **a)** Rostral to caudal extent of phrenic MN dendrites, as revealed by dil injections into the phrenic
519 nerve in control and $\beta\gamma$ -cat MNA mice. Scale bar= 100 μ m. **b-d)** Radial plot of the normalized
520 fluorescent intensity in each octant in control (b, d) and $\beta\gamma$ -cat MNA (c-d) mice. Zero degrees
521 represents a line through the center of the phrenic MN cell bodies that is perpendicular to the
522 midline. Dendrites in $\beta\gamma$ -cat MNA mice shift ventrally, with a loss of dorsolateral projections. **e)**
523 Quantification of the proportion of dendritic fluorescent intensity from 0 to 90 degrees (left,
524 dorsolateral) and from 180 to 225 degrees and 315 to 360 degrees (right, ventral) in control and
525 $\beta\gamma$ -cat MNA mice.

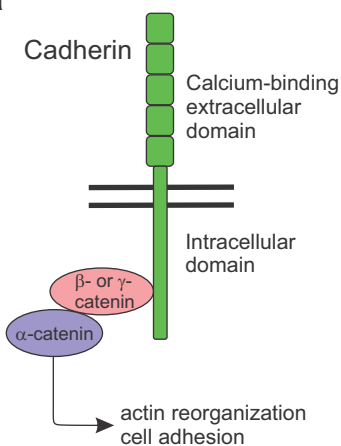
526 **Figure 5. Catenins regulate phrenic MN axonal arborization**

527 **a)** Diaphragm innervation in control and $\beta\gamma\text{-cat}^{\text{MNA}}$ mice. $\beta\gamma\text{-cat}^{\text{MNA}}$ mice display a reduction in
528 ventral diaphragm innervation (arrow) and arborization complexity (star) at e18.5. Motor axons
529 are labeled in green (combination of neurofilament light chain/synaptophysin) and
530 neuromuscular junctions in red (α -bungarotoxin, btx). Scale bar= 500 μm . **b)** Phrenic projections
531 were traced and quantified in ImageJ. **c)** Quantification of diaphragm innervation in control and
532 $\beta\gamma\text{-cat}^{\text{MNA}}$ mice.

533 **Figure 6. A narrow temporal requirement for catenin signaling in phrenic MN topography
534 and function.**

535 **a)** Examples of phrenic MN cell body distribution in control and $\beta\gamma\text{-cat}^{\text{ChATMNA}}$ mice at e13.5.
536 *ChAT*::*Cre*-mediated catenin deletion from postmitotic MNs does not affect their position or
537 clustering. Scale bar= 25 μm . **b)** *dil* injections into the phrenic nerve reveal similar dendritic
538 architecture in control and $\beta\gamma\text{-cat}^{\text{ChATMNA}}$ mice at e18.5. Scale bar= 100 μm . **c)** Representative
539 suction electrode recordings from the phrenic nerve in P4 control and $\beta\gamma\text{-cat}^{\text{ChATMNA}}$ mice show
540 similar levels of phrenic MN activation. **d)** Burst frequency, duration and integrated activity are
541 unchanged in $\beta\gamma\text{-cat}^{\text{ChATMNA}}$ mice (n=7 control, n=7 $\beta\gamma\text{-cat}^{\text{ChATMNA}}$ mice).

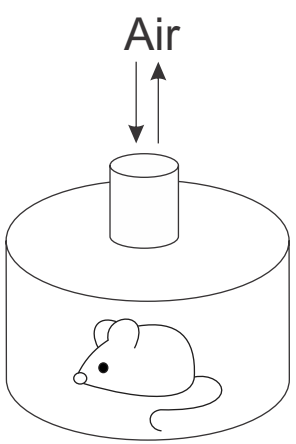
a



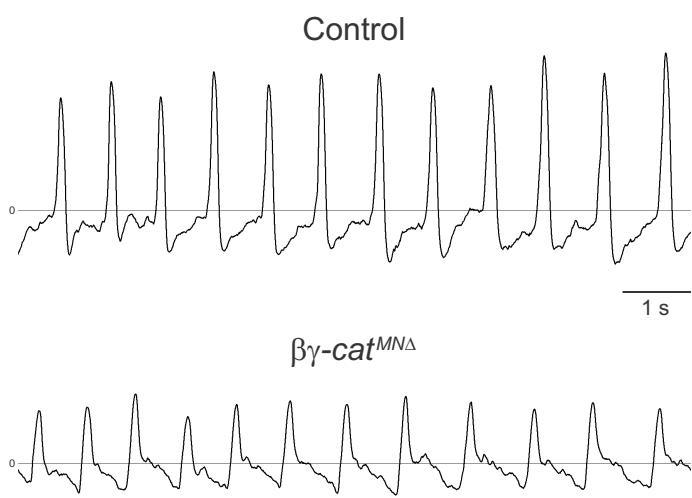
b



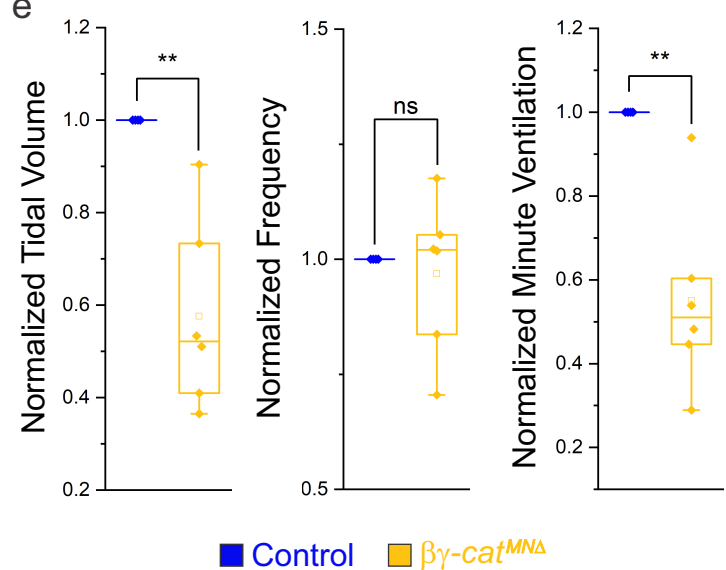
c



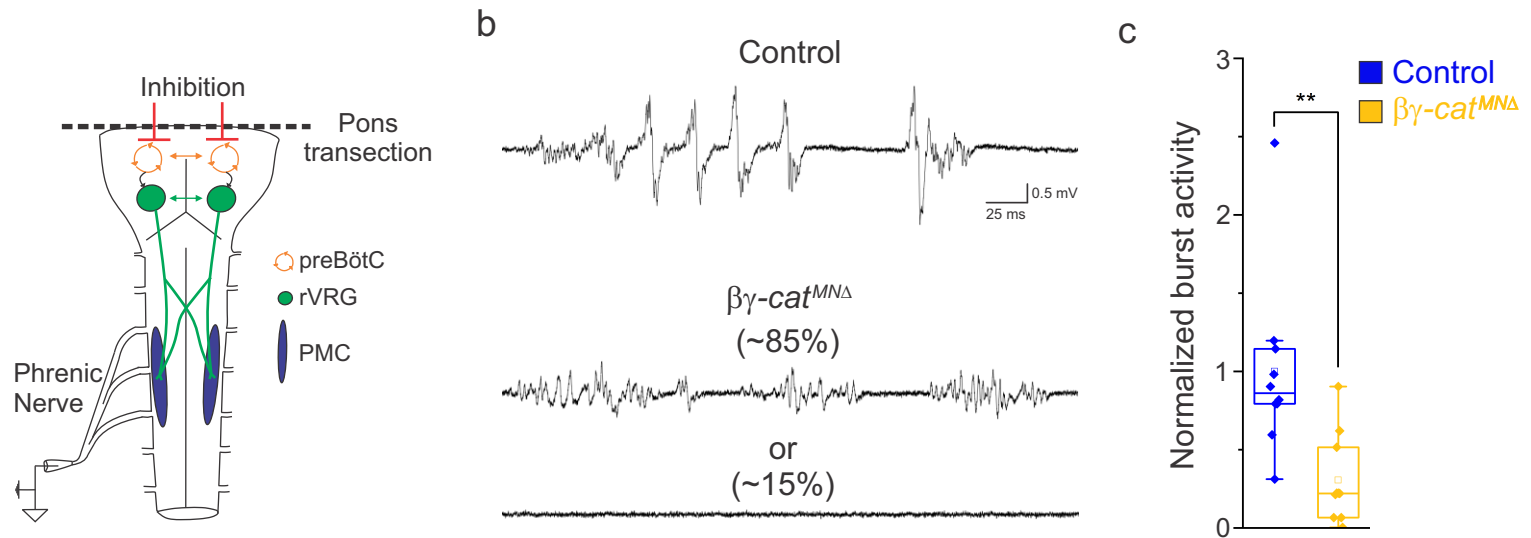
d



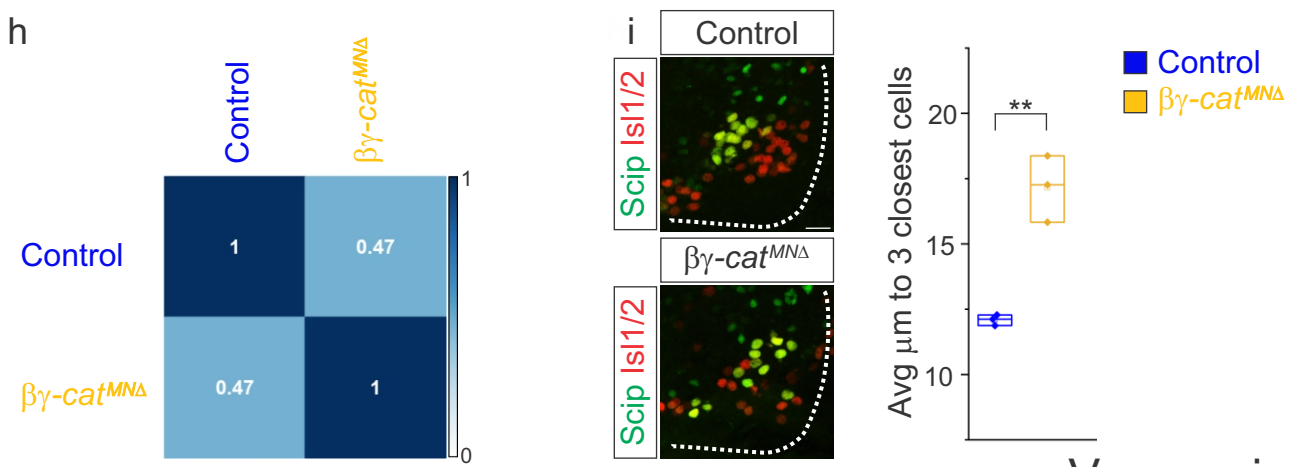
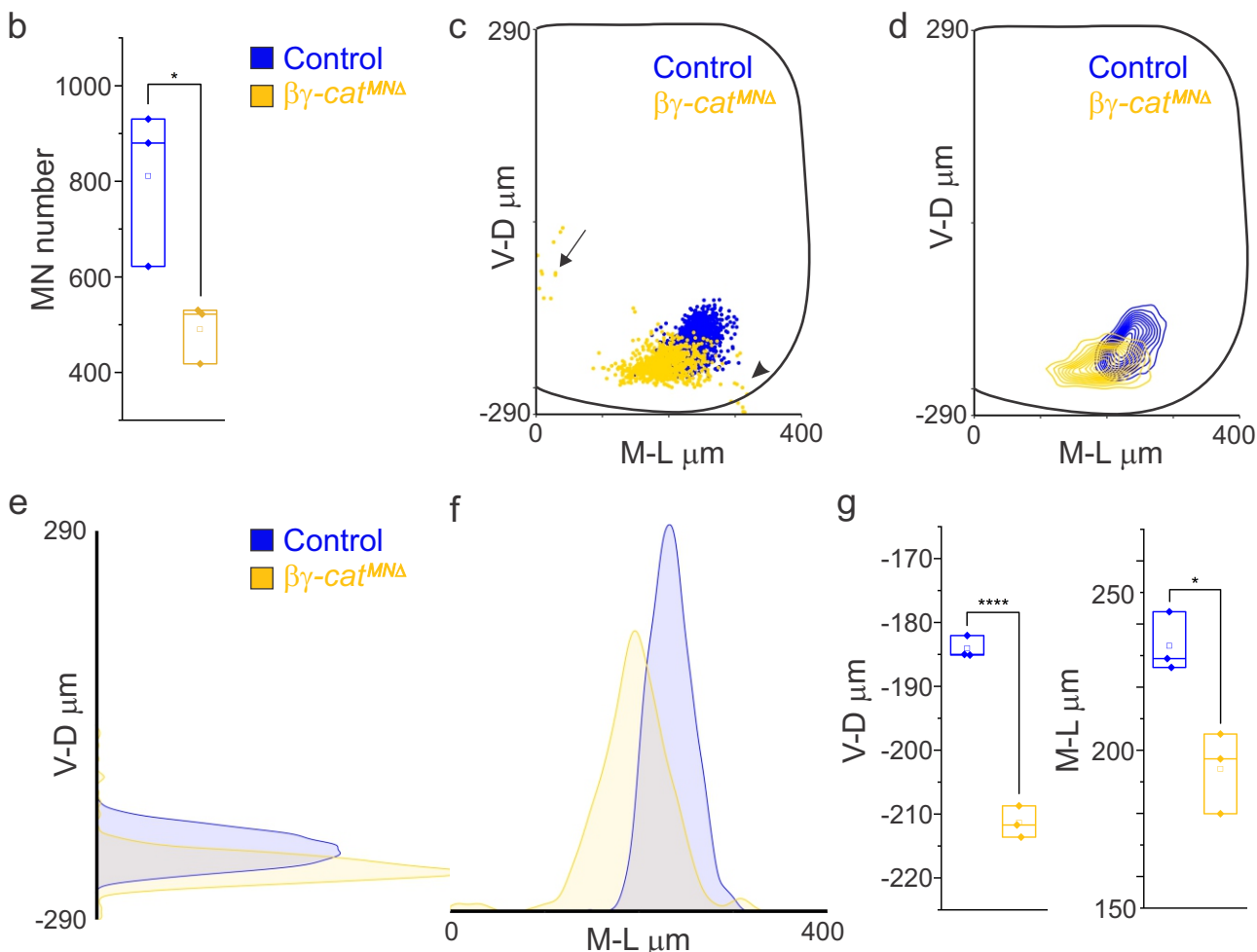
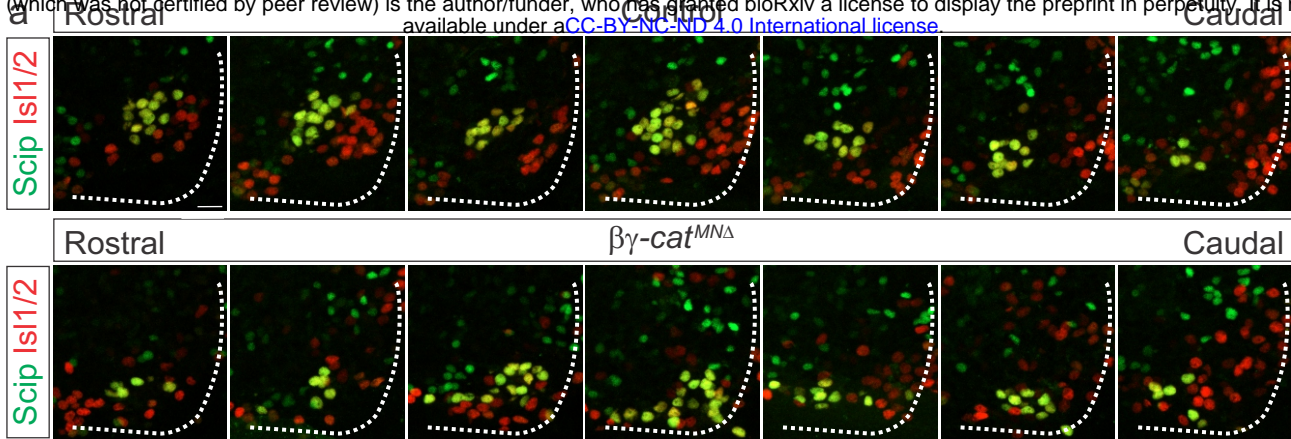
e

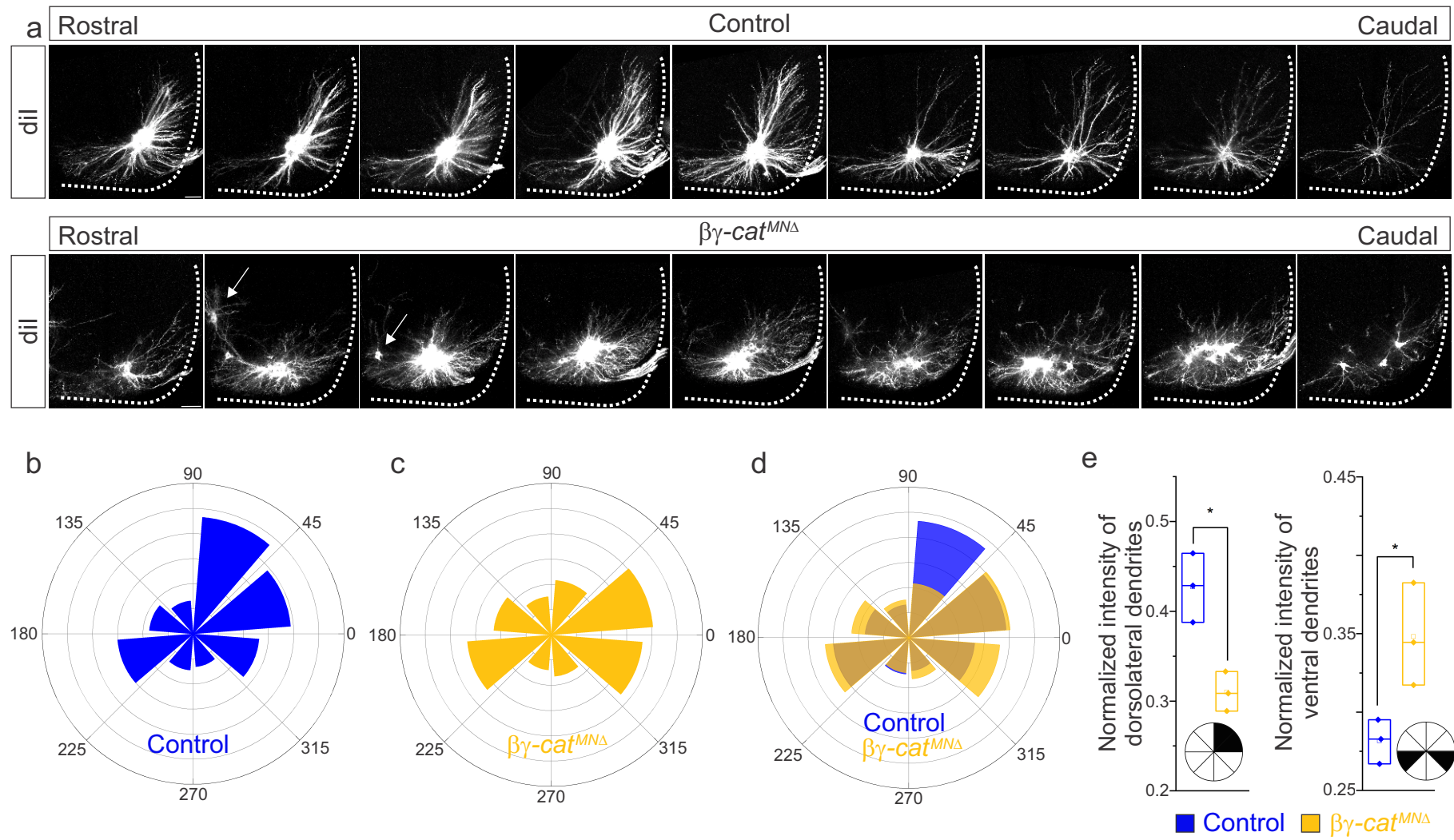


Vagnozzi_Figure 1

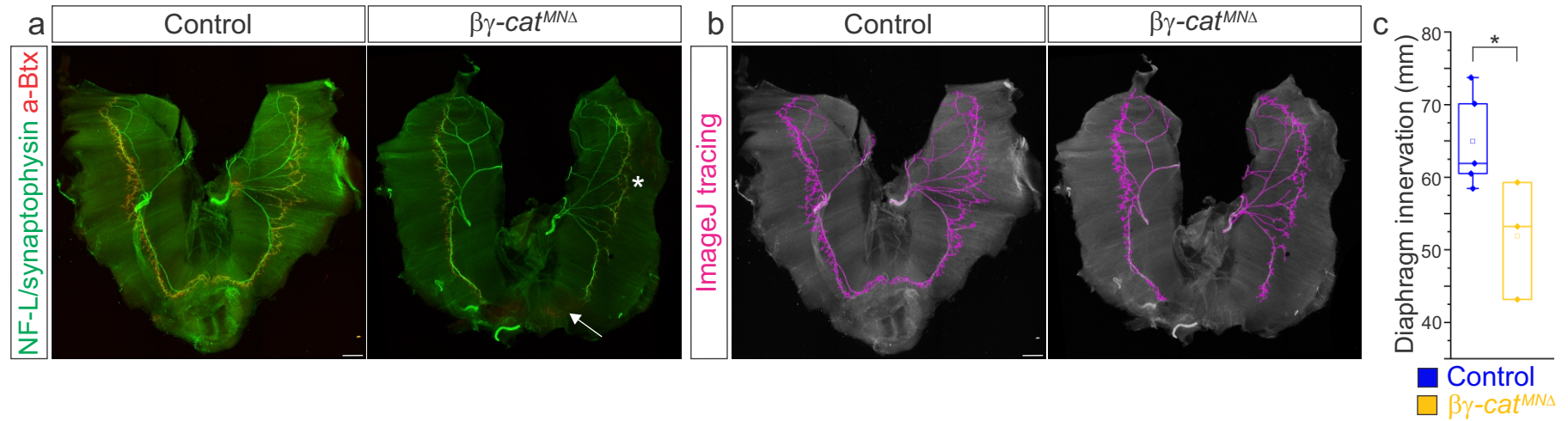


Vagnozzi_Figure 2





Vagnozzi_Figure 4



Vagnozzi_Figure 5

